

**KINETICS OF OXIDE FORMATION ON VARIOUS METAL SURFACES IN
THE PRESENCE OF OXYGEN-NITROGEN MIXTURES**



Sarita Weerakul

A Thesis Submitted in Partial Fulfilment of the Requirements
for the Degree of Master of Science
The Petroleum and Petrochemical College, Chulalongkorn University
in Academic Partnership with
The University of Michigan, The University of Oklahoma,
Case Western Reserve University and Institut Français du Pétrole
2012


I 28373686


Thesis Title: Kinetics of Oxide Formation on Various Steel Surfaces in the Presence of Oxygen-Nitrogen Mixtures
By: Sarita Weerakul
Program: Petrochemical Technology
Thesis Advisors: Assoc. Prof. Thirasak Rirksomboon
Prof. Frank R. Steward

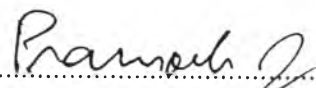
Accepted by The Petroleum and Petrochemical College, Chulalongkorn University, in partial fulfilment of the requirements for the Degree of Master of Science.



..... College Dean
(Asst. Prof. Pomthong Malakul)

Thesis Committee:


.....
(Assoc. Prof. Thirasak Rirksomboon)


.....
(Prof. Frank R. Steward)


.....
(Assoc. Prof. Pramoch Rangsunvigit)


.....
(Dr. Boonrod Sajjakulnukit)

บทคัดย่อ

สรिता วีระกุล : ไคเนติกส์ของการเกิดออกไซด์บนผิวโลหะชนิดต่างๆ ภายใต้สภาวะที่มีออกซิเจน และไนโตรเจน (Kinetics of Oxide Formation on Various Steel Surfaces in the Presence of Oxygen-Nitrogen Mixtures) อ. ที่ปรึกษา: รศ.ดร. ชिरศักดิ์ ฤกษ์สมบูรณ์ และ ศ.ดร. แฟรงค์ อาร์. สจิว์วต์, 86 หน้า

งานวิจัยนี้ได้ศึกษาการก่อตัวของออกไซด์บนผิวโลหะชนิดต่างๆ ที่อุณหภูมิ 400 และ 90 องศาเซลเซียส ตัวอย่างโลหะที่ใช้ได้แก่ เหล็กคาร์บอน (CS A106B) เหล็กสแตนเลส (SS 316) และนิกเกิลอัลลอยด์ (Alloy 625) ในสภาวะที่ความเข้มข้นของออกซิเจนต่างๆ จากการศึกษาการก่อตัวของออกไซด์บนเหล็กคาร์บอนที่อุณหภูมิ 400 องศาเซลเซียสพบว่า ออกไซด์ที่เกิดขึ้นในสภาวะที่ความเข้มข้นของออกซิเจนคงที่คือฮีมาไทท์ (Fe_2O_3) ส่วนออกไซด์ที่เกิดขึ้นในสภาวะที่มีการเปลี่ยนแปลงความเข้มข้นของออกซิเจนนั้นพบว่ามีส่วนฮีมาไทท์ (Fe_2O_3) และแมกนีไทท์ (Fe_3O_4) โดยสามารถคำนวณความหนาของชั้นออกไซด์ที่เกิดขึ้นได้จากน้ำหนักที่เพิ่มขึ้นบนโลหะตัวอย่าง เพื่อนำไปใช้ในการสร้างแบบจำลองของอัตราการเกิดออกไซด์บนผิวโลหะแต่ละชนิด ทั้งนี้พบว่าอัตราการเกิดออกไซด์บนผิวเหล็กคาร์บอนที่ 400 องศาเซลเซียสนั้น ถูกควบคุมโดยอัตราการแพร่ของออกซิเจนผ่านชั้นออกไซด์ ได้ทำการคำนวณค่าการแพร่ของออกซิเจนผ่านชั้นออกไซด์และนำไปใช้ในการทำนายอัตราการผลิตของออกไซด์ในสภาวะที่มีการเปลี่ยนแปลงความเข้มข้นของออกซิเจน จากการศึกษาการเกิดออกไซด์บนผิวเหล็กสแตนเลสและนิกเกิลอัลลอยด์พบว่าเกิดชั้นออกไซด์ที่บางมาก โดยไม่มีผลต่อการเพิ่มขึ้นของน้ำหนักของโลหะตัวอย่างอย่างมีนัยสำคัญ นอกจากนี้ได้ศึกษาการเกิดของออกไซด์บนพื้นผิวเหล็กคาร์บอนและเหล็กสแตนเลสที่อุณหภูมิ 90 องศาเซลเซียส พบว่าไม่มีชั้นออกไซด์เกิดขึ้น และไม่เกิดการเปลี่ยนแปลงของน้ำหนักของตัวอย่างอย่างมีนัยสำคัญ

ABSTRACT

5371020063: Petrochemical Technology Program

Sarita Weerakul: Kinetics of Oxide Formation on Various Steel Surfaces in the Presence of Oxygen-Nitrogen Mixtures.

Thesis Advisors: Assoc. Prof. Thirasak Rirksomboon. Prof. Frank R. Steward

Keywords: Kinetics of oxide formation/ Oxidation of metal/ Diffusion of oxygen through oxide films/Corrosion monitoring

The formation of oxides at 400°C and 90°C with different oxygen concentration conditions on various metal surfaces; carbon steel, stainless steel and nickel-alloy was studied. From 400°C tests of carbon steel surfaces, oxide films were observed in both conditions; the oxide formed on the surfaces which were exposed to an atmosphere with no change in O₂ concentration was Hematite. On the surfaces which were exposed to an atmosphere with changing O₂ concentration, Magnetite and Hematite were found due to the different conditions of apparatus used. The thickness of the oxide film formed on each membrane was calculated from the weight gained by the membrane and the kinetics of oxide formation on each condition was modelled. From the experiment of carbon steel at 400 °C exposure, the reaction rate was controlled by diffusion of O₂ through the oxide layer. The diffusivity of oxygen through the oxide layer, D_{O_2} , was calculated from the rate of oxide formation on the surfaces which were exposed to an atmosphere with no change in O₂ concentration and was found that $D_{O_2} = 7.05545 \times 10^{-14} m^2 / s$ and the parabolic rate, $k_p = 1.089 \times 10^{-17} m^2 / s$. D_{O_2} was used in the prediction of oxide form in the atmosphere with changing O₂ concentration. The layer of oxide formed on stainless steel and nickel-alloy surfaces, however, was very thin and the weight gains on these metals were not significant. Carbon steel and stainless steel were also tested at 90°C, weight gains on these membranes were not significant and no oxide films were observed.

ACKNOWLEDGEMENTS

It is my honour to study a master's degree at the Petroleum and Petrochemical College, Chulalongkorn University and became a Graduate Exchange Student at University of New Brunswick. The completion of this research would not have been possible without the assistance and support of many people in Thailand and Canada. The researcher would like to acknowledge the assistance and support of people who have supported this research.

I would like to thank my supervisor Prof. Frank R. Steward for his guidance, kind help, support, and patience throughout the whole time of the research, also Prof. D. H. Lister, A. Feicht and C. Kongvarhodom for their helpful discussion and suggestion. I am also grateful to Assoc. Prof. Thirasak Rirksomboon who gave me an opportunity to carry out my research at the University of New Brunswick as an exchange student.

Without the following persons, I could not have performed many analyses, Dr. Lihui Liu, and Dr. Suporn Boonsue, who helped me in analyzing my samples and giving me useful information and suggestions about my results. Steven R. Cogswell also deserves thanks for their effort in the SEM work.

Furthermore, I would like to express my gratitude to all my friends and colleagues at the Centre for Nuclear Energy Research (CNER) for providing the laboratory facilities, and their enormous support and expertise.

Last but not the least, I wish to give my deepest gratitude to my beloved family for their unconditional love, and constant encouragement throughout the successful completion of this research.

The author is grateful for the scholarship and funding of the thesis work provided by the Centre for Nuclear Energy Research, University of New Brunswick, Canada and the Petroleum and Petrochemical College; and the National Center of Excellence for Petroleum, Petrochemicals, and Advanced Materials, Thailand.

TABLE OF CONTENTS

	PAGE
Title Page	i
Abstract (in English)	iii
Abstract (in Thai)	iv
Acknowledgements	v
Table of Contents	vi
List of Tables	x
List of Figures	xi
 CHAPTER	
I INTRODUCTION	1
 II THEORETICAL BACKGROUND AND LITERATURE REVIEW	
2.1 Corrosion of Steel	3
2.1.1 Flow Accelerated Corrosion (FAC)	3
2.2 Mechanism of Oxide Growth and Hydrogen Evolution in Corrosion	4
2.3 Hydrogen Probe for Monitoring Corrosion	7
2.3.1 Hydrogen Probe Principle	7
2.3.2 Hydrogen Effusion Probe (HEP)	9
2.4 Fundamental Law of Diffusion for Hydrogen	12
2.4.1 Sievert's Law	12
2.4.2 Mechanism of Hydrogen Transport Through Metals	14
2.4.3 Hydrogen Diffusivity in Oxide Films	16
2.5 Iron Oxides	17
2.5.1 Thermodynamics of the Fe-O System	20
2.5.2 Stability of Iron Oxide	23

CHAPTER	PAGE
2.5.3 Oxidation Mechanism of Iron	26
2.5.4 Formation and Transformation of Iron Oxide	27
2.5.5 Oxidation of Magnetite to Maghemite or Hematite	28
2.5.6 Kinetics of High Temperature Oxidation/Corrosion of Iron in Gases	29
2.5.7 Effect of Alloying Elements on Oxidation Rates	32
2.5.7.1 Effect of Carbon	32
III EXPERIMENTAL	33
3.1 Materials and Equipment	33
3.1.1 Materials	33
3.1.2 Equipments	33
3.2 Apparatus Set-up	34
3.3 Experimental Procedure	35
3.3.1 Surface Preparation	35
3.3.1.1 Stamping Membranes	35
3.3.1.2 Polishing Sample Surfaces	36
3.3.2 Test Matrix and Extra Surface Required	36
3.3.3 Preconditioning Components	38
3.3.4 Testing Procedure	38
3.4 Sample Analysis	39
IV RESULTS AND DISCUSSION	40
4.1 Materials Characterization	40
4.1.1 Baseline Analysis	40
4.1.2 Carbon Steel (CS A106B)	43
4.1.2.1 Thermodynamic Equilibrium	48

CHAPTER	PAGE
4.1.3 Stainless Steel (SS 316)	51
4.1.4 Nickel Alloy (Alloy 625)	52
4.2 Weight Gain on Samples and Thickness of Oxide Layers	54
4.3 Kinetics of Oxide Formation	59
4.3.1 Diffusion of Oxygen Through Oxide Layer Control	60
4.3.1.1 If Magnetite was Formed	60
4.3.1.2 If Hematite was Formed	62
4.3.2 Chemical Reaction Control	63
4.3.2.1 If Magnetite was Formed	63
4.3.2.1 If Hematite was Formed	64
4.3.3 Kinetics of Oxide Formation on Carbon Steels Exposed to an Atmosphere with No Change in O ₂ Concentration (B-side)	65
4.3.4 Kinetics of Oxide Formation on Carbon Steels Exposed to an Atmosphere with Change in O ₂ Concentration (A-side)	67
4.3.4.1 Kinetics of Oxide Formation in Experimental Set 1 (A-side-1)	67
4.3.4.2 Kinetics of Oxide Formation in Experimental Set 2 (A-side-2)	71
V CONCLUSIONS AND RECOMMENDATIONS	75
5.1 Conclusions	75
5.1.1 Carbon Steel (CS A106B)	75
5.1.2 Stainless Steel (SS 316) and Nickel-alloy (Alloy 625)	76
5.2 Recommendations	76

	PAGE
REFERENCES	77
APPENDICES	80
Appendix A Cavity Volume and Amount of Oxygen in Each Test Section	80
Appendix B Raman Spectra of Each Wire in Table A1 and Table A2	83
CURRICULUM VITAE	87

LIST OF TABLES

TABLE	PAGE
2.1 The iron oxides (Cornell and Schwertmann 2003)	17
2.2 Standard free energies, enthalpies and entropies of formation of iron oxides at 0.1 MPa and 298 K (Cornell and Schwertmann 2003)	22
2.3 Standard free energies, enthalpies and entropies for soluble Fe and some other species at 298 K (Cornell and Schwertmann 2003)	23
2.4 Interconversions among the iron oxides (Cornell and Schwertmann 2003)	28
3.1 Test matrix	37
3.2 Extra polished surface requirement	38
4.1 Elemental analysis results of baseline samples (membranes)	42
4.2 Elemental analysis results of extra surface samples (wires)	43
4.3 Data for reaction $4Fe_3O_4 + O_2 \rightleftharpoons 6Fe_2O_3$	49
4.4 Equilibrium constant and partial pressure of oxygen at equilibrium for various temperatures	50
4.5 Comparison between the thickness of oxide layer on carbon steel membrane (CS A106B) from calculation and from average cross-sectional analysis	56
A1 Cavity volume and amount of oxygen in experimental set 1	81
A2 Cavity volume and amount of oxygen in experimental set 2	82

LIST OF FIGURES

FIGURE	PAGE
2.1 Mechanism of flow accelerated corrosion and wall thinning induced by FAC (http://afre.qse.tohoku.ac.jp/research/FAC/e-index.html).	4
2.2 Schematic of the double oxide layer formed on carbon steel (Lister, Slade et al. 1997).	5
2.3 Schematic view of the formation of the magnetite film on the steel surface in high temperature water (Cheng and Steward 2004).	6
2.4 Schematic of HEP assembly (McKeen, Lalonde et al. 2007).	10
2.5 The HEP (top) and FOLTM (bottom) installed on feeder pipe at PLGS (McKeen, Lalonde et al. 2007).	11
2.6 Diffusion of hydrogen through iron; Borelius and Lindblom (Smithells and Ransley 1935).	14
2.7 Seven steps of hydrogen permeation (Stone 1981).	15
2.8 Micaceous hematite from Western Australia (Courtesy R. Giovanoli, referenced in <i>The Iron Oxides: Structure, Properties, Reactions, Occurrences and Uses</i>).	18
2.9 Crystal forms of platy and rhombohedral hematite (Courtesy H. Stanjek, referenced in <i>The Iron Oxides: Structure, Properties, Reactions, Occurrences and Uses</i>).	19
2.10 Crystal forms of magnetite a), c) octahedron; b) rhombodecahedron; d) twin. (Kostov, 1968, referenced in <i>The Iron Oxides: Structure, Properties, Reactions, Occurrences and Uses</i>).	19
2.11 Equilibrium phase diagram for the iron-oxygen system (Hansen, Anderko et al. 1965).	24

FIGURE	PAGE
2.12 Phase diagram of the Fe-O system (Bogbandy & Engell, 1971, referenced in The Iron Oxides: Structure, Properties, Reactions, Occurences and Uses).	25
2.13 The iron-oxygen phase diagram (Kofstad 1988).	25
2.14 The Ellingham/Richardson diagram for iron oxides (Gaskell 1981).	26
2.15 Schematic representation of oxide layer growth on iron: (a) chemisorption of oxygen; (b) the formation of a fine mosaic layer; (c) growth of the oxide crystal; (d) appearance of the second layer (Gulbransen and Ruka 1952).	27
2.16 Schematic representation of oxidation of iron. P = plane of growth (West, 1980, referenced in The Iron Oxides: Structure, Properties, Reactions, Occurences and Uses).	30
2.17 Plots of the growth laws of oxidation: a) parabolic, b) rectilinear, c) quasi-rectilinear, d) logarithmic (West, 1980, referenced in The Iron Oxides: Structure, Properties, Reactions, Occurences and Uses).	31
3.1 Apparatus with one membrane assembly.	34
3.2 Schematic of the constructed HEP instrument.	35
3.3 Stamp example.	36
4.1 SEM image of baseline surfaces; a) carbon steel, b) stainless steel and c) nickel-alloy.	41
4.2 SEM images of B-side carbon steels exposed to the free air; a) 1 day, b) 7 days and c) 14 days.	44
4.3 Raman spectra of B-side carbon steels exposed to the free air for 1 day (CS-1(B)), 7 days (CS-7(B)) and 14 days (CS-14(B)).	44

FIGURE	PAGE
4.4 SEM images of A-side carbon steels in the first set of experiments exposed to the simulated environment; a) 1 day, b) 7 days and c) 14 days.	45
4.5 Raman spectra of A-side carbon steels in the first set of experiments exposed to the simulated environment for 1 day (CS-1(A)), 7 days (CS-7(A)) and 14 days (CS-14(A)).	45
4.6 SEM images of A-side carbon steels in the second set of experiments exposed to the simulated environment; a) 5 hours, b) 1 day and c) 7 days.	46
4.7 Raman spectra of A-side carbon steels in the second set of experiments exposed to the simulated environment for 5 hours (CS-5hr(A2)), 1 day (CS-1(A2)) and 7 days (CS-7(A2)).	47
4.8 SEM images of carbon steel surfaces exposed to 90°C for; a) 1 day, b) 7 days and c) 14 days.	47
4.9 SEM images of stainless steel surface exposed to 400°C for 14 days.	51
4.10 EDS spectra of stainless steel surface after the 400°C exposure.	52
4.11 SEM images of nickel-alloy surfaces exposed to 400°C for 14 days.	53
4.12 EDS spectra of nickel-alloy surface after the 400°C exposure.	53
4.13 Relation between the weight gain per unit area and exposure time for the 400°C exposure samples.	54
4.14 Relation between the thickness of oxide layer and exposure time for the 400°C exposure samples.	55
4.15 Cross-sectional image of the carbon steel membrane (B-side) exposed to 400°C for 1 day.	56

FIGURE	PAGE
4.16 Cross-sectional image of the carbon steel membrane (A-side) exposed to 400°C for 1 day.	57
4.17 Cross-sectional image of the carbon steel membrane (B-side) exposed to 400°C for 7 days.	57
4.18 Cross-sectional image of the carbon steel membrane (A-side) exposed to 400°C for 7 days.	58
4.19 Cross-sectional image of the carbon steel membrane (B-side) exposed to 400°C for 14 days.	58
4.20 Cross-sectional image of the carbon steel membrane (A-side) exposed to 400°C for 14 days.	59
4.21 Schematic of iron oxide formed on iron surface.	59
4.22 Relation between x or x^2 and exposure time for B-side in the 400°C exposure samples.	65
4.23 The plot of oxide layer thickness versus time of carbon steel (A-side-1).	69
4.24 Relations between concentrations of air and oxygen inside the cavity and exposure time of the set 1 experiment.	70
4.25 Relations between pressure inside the cavity and exposure time of the set 1 experiment.	70
4.26 The plot of oxide layer thickness versus time of carbon steel (A-side-2).	73
4.27 Relations between concentrations of air and oxygen inside the cavity and exposure time of the set 2 experiment.	74
4.28 Relations between pressure inside the cavity and exposure time of the set 2 experiment.	74
B1 Raman spectra of wire in run 7.	83
B2 Raman spectra of WIRE-01.	83
B3 Raman spectra of WIRE-02.	84
B4 Raman spectra of WIRE-03.	84

FIGURE		PAGE
B5	Raman spectra of WIRE-05.	85
B6	Raman spectra of WIRE-07.	85
B7	Raman spectra of WIRE-11.	86